

Generative Modelling of BRDF Textures from Flash Images

PHILIPP HENZLER, University College London, United Kingdom

VALENTIN DESCHAINTE, Imperial College London, United Kingdom

NILOY J. MITRA, University College London and Adobe Research, United Kingdom

TOBIAS RITSCHER, University College London, United Kingdom

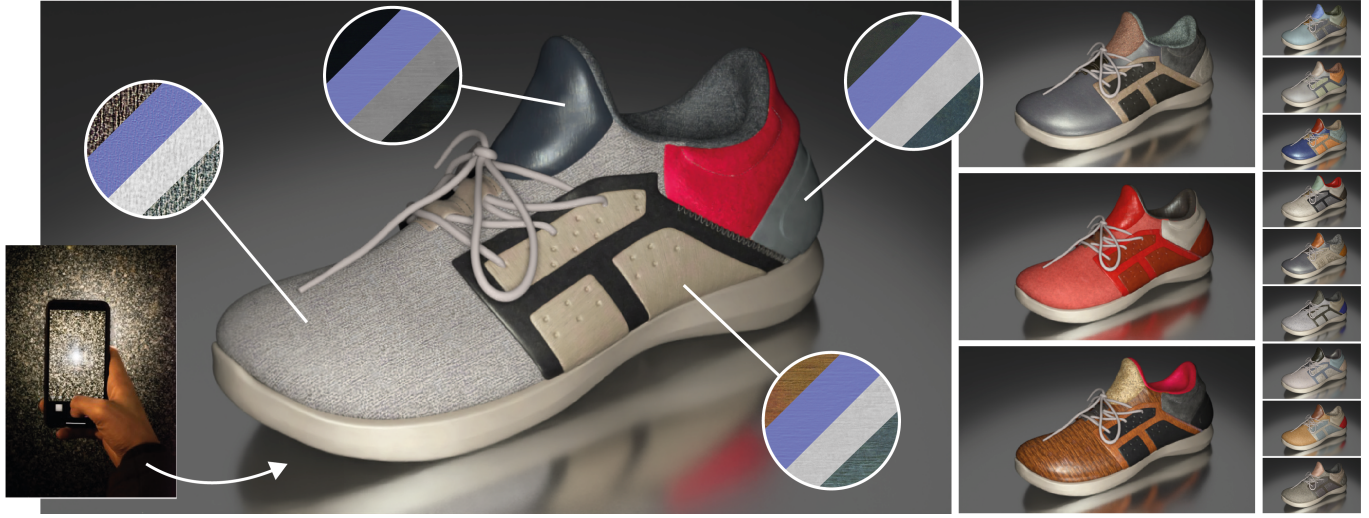


Fig. 1. Random samples from our generative model of BRDF maps (e.g., circular insets), assigned to a 3D object of a shoe. Training samples were obtained using flash images. Our model reveals a BRDF material space that can be sampled from, projected to, and interpolated across.

We learn a latent space for easy capture, semantic editing, consistent interpolation, and efficient reproduction of visual material appearance. When users provide a photo of a stationary natural material captured under flash light illumination, it is converted in milliseconds into a latent material code. In a second step, conditioned on the material code, our method, again in milliseconds, produces an infinite and diverse spatial field of BRDF model parameters (diffuse albedo, specular albedo, roughness, normals) that allows rendering in complex scenes and illuminations, matching the appearance of the input picture. Technically, we jointly embed all flash images into a latent space using a convolutional encoder, and – conditioned on these latent codes – convert random spatial fields into fields of BRDF parameters using a convolutional neural network (CNN). We condition these BRDF parameters to match the visual characteristics (statistics and spectra of visual features) of the input under matching light. A user study confirms that the semantics of the latent material space agree with user expectations and compares our approach favorably to previous work.

Project webpage: <https://henzler.github.io/publication/neuralmaterial/>.

1 INTRODUCTION

Rendering realistic images for feature films or computer games requires adequate simulation of light transport. Besides geometry and illumination, an important factor is material appearance.

Authors' addresses: Philipp Henzler, Department of Computer Science, University College London, United Kingdom, p.henzler@cs.ucl.ac.uk; Valentin Deschaintre, Imperial College London, United Kingdom, v.deschaintre@imperial.ac.uk; Niloy J. Mitra, University College London and Adobe Research, United Kingdom, n.mitra@ucl.ac.uk; Tobias Ritscher, Department of Computer Science, University College London, United Kingdom, t.ritschel@ucl.ac.uk.

Material appearance has three aspects of variation: First, when view or light direction change, reflected light changes. The physics of this process are well-understood and can be simulated provided the input parameters are available. Second, behavior changes across materials. For example, leather reacts differently to light or view changes than paper would, yet, different forms of leather clearly share visual properties, i.e., form a (material) space. Third, appearance details depend on spatial position. Different locations in one leather exemplar behave differently but share the same visual statistics [Portilla and Simoncelli 2000], i.e., they form a *texture*.

Classic computer graphics captures appearance by *reflection models*, which predict for a given i) light-view configuration, ii) material, and iii) spatial position, how much light is reflected. Typically, the first variation (light and view direction) is covered by *BRDF models*, analytic expressions, such as Phong [1975] which map the light and view direction vector to scalar reflectance. The second variation (material) is covered by choosing *BRDF model parameters*, such as Phong glossiness. In practice, it can be difficult, given a desired appearance, to choose those parameters e.g., how to make a leather look more like fabric. Measuring BRDF model parameters requires complex capture hardware. The third variation (spatial) is addressed by storing multiple BRDF model parameters in images of finite size – often referred to as Spatially-varying Bi-directional Reflectance Distribution Function (svBRDF) maps – or writing functional expressions to reproduce their behaviour. It is even more

challenging to choose these parameters to produce something coherent like leather, in particular over a large or even infinite spatial extent. Additionally, storing all these values requires substantial memory and programming functional expressions to mimic their statistics requires expert skills and time. Capturing the spatial variation of BRDF model parameters over space using sensors is even more involved [Schwartz et al. 2013].

Addressing those issues, we provide a reflectance model to jointly generalize across all of these three axes. Instead of using analytic parameters, we parametrize appearance by latent codes from a learned space, allowing for generation, interpolation and semantic editing. Without involved capture equipment, these codes are produced by presenting the system a simple 2D flash image, which is then embedded into the latent space. Avoiding to store any finite image texture, we learn a second mapping to produce svBRDF maps from the infinite random field (noise) on-the-fly, conditioned on the latent material code. Instead of using any advanced capture device for learning, flash images will be the only supervision we use.

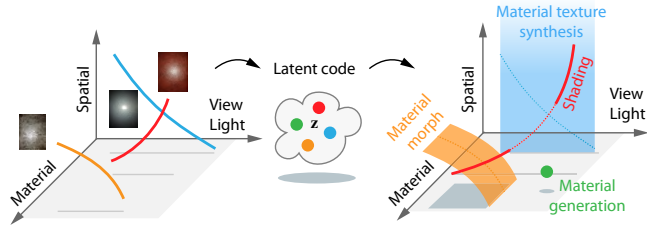


Fig. 2. **BRDF space.** From a flash image, which contains sparse observations across material, space and view-light (**left**) we map to a latent code (**middle**) so that changes in that code can be decoded to enable (**right**) material synthesis (holding material fixed and moving spatially), material morphing (holding space and view/light fixed and changing material), or classical shading and material generation (points in the latent space).

A use case of our approach is shown in Fig. 1. First, a user provides a “flash image”, a photo of a flat material sample under flash illumination. This sample is embedded as a code into a latent space using a CNN. This code is a very compact description that can be manipulated, e.g., interpolated with a different material or changed along semantic axis. Previous work has considered spaces of BRDFs [Matusik 2003] or RGB textures [Matusik et al. 2005] but no spatial variation of reflectance. Conditioned on this code, a second CNN can generate an infinite field of BRDF to be directly used in rendering.

For training, we solely rely on real flash images. The key insight, inspired by Aittala et al. [2016] is that these flash images reveal the same material at different image locations – they are stationary – but under different view and light angles. Using this constraint, Aittala et al. [2016] were able to decompose a single input image to capture the parameters of a material model that could then be rendered under novel view or light directions. However, this covers only part of the generalization we are targeting: it generalizes across view and light, but not across location or material. Further, they require performing an optimization for every exemplar, requiring time in the order of hours, while ours requires milliseconds only.

In summary, our main contributions are

- a generative model of a BRDF material texture space;
- generation of maps that are diverse over the infinite plane;
- a flash image dataset of materials enabling our training with no BRDF parameter supervision or synthetic data; and
- feed-forward embedding of exemplar flash images into the space in milliseconds using a CNN, without per-material optimization.

Our implementation will be publicly available upon acceptance.

2 PREVIOUS WORK

Our work has background in texture analysis, appearance modelling and design spaces.

2.1 Textures in Graphics

A classic definition of texture is defined by Julesz [1965]: *a texture is an image full of features that in some representation have the same statistics*. Portilla and Simoncelli [2000] have provided a practical method to compute representations in to do statistics on. They use linear filters on multiple scales

Perlin [1985] was first to capture the fractal [Mandelbrot 1983] stochastic variation of appearance in model applicable to Computer Graphics. His approach is simple – a linear combination of noise at different scales – yet extremely powerful, and has led to extensive use in computer games or production rendering. Wavelet noise [Cook and DeRose 2005] moved this idea further by band-limiting the noise that is combined. Such methods can be used of materials, e.g., for gloss maps, bump maps, etc. Regrettably, it does not provide a solution to acquire a texture from an exemplar, which is left to manual adjustment.

To generate textures from exemplars, non-parametric sampling [Efros and Leung 1999], vector quantization [Wei and Levoy 2000], optimization [Kwatra et al. 2005] or nearest-neighbour field synthesis (PatchMatch [Barnes et al. 2009]) have been proposed. These are used less in production rendering or games, due to issues in computational scalability and lack of intuitive control.

The word “texture” can be ambiguous to mean stochastic variation, as well as images attached on surfaces to localize color features. Here, we focus on stochastic variation in the sense of Julesz [1965] or Portilla and Simoncelli [2000].

Our approach will build on deep learning-based texture synthesis [Bergmann et al. 2017; Gatys et al. 2015; Johnson et al. 2016; Karras et al. 2019; Sendik and Cohen-Or 2017; Shaham et al. 2019; Simonyan and Zisserman 2014; Ulyanov et al. 2016, 2017; Zhou et al. 2018]. Besides applying them to BRDFs, we extend these ideas. We detail their background in Sec. 3.2

2.2 Material Modeling

Representing appearance in simulation-based graphics has been an activate research field for decades. The survey by Guarnera et al. [2016] present detailed discussion of the many different material model and BRDF acquisition approach. In our method, we use a state-of-the-art micro-facet BRDF model [Cook and Torrance 1982], and focus on deep-learning based material modelling and acquisition.

Many methods have been proposed to acquire materials using data-driven approaches. Matusik [2003] proposed a data driven

BRDF model, using a linear model. More recently, Rematas et al. [2016] extract reflectance maps from 2D images using a CNN trained in a supervised manner. Materials and illuminations acquisition were further explored by Georgoulis et al. [2017]. Deschaintre et al. [2018] proposed a rendering loss to capture svBRDFs from flash images. Pix2Pix [Isola et al. 2016] inspired many other approaches for image to image translation to translate RGB pixels to material attributes [Li et al. 2017, 2018a,b]. Most work now includes a differentiable shading step [Deschaintre et al. 2018, 2019; Guo et al. 2020; Li et al. 2018b; Liu et al. 2017] such as we do here. Gao et al. [2019] proposed to use a post-optimization in an encoded latent space, improving an initial material estimation, and comparing renderings of their results directly to their input pictures. All these approaches focus on capturing a single instance of a svBRDF map, but with little or no editing options across materials (semantic space) or generalization across the spatial domain (diversity). Kuznetsov et al. [2019] modeled an important aspect of physically-based rendering using adversarial training: the Normal Distribution Function (NDF). We take key inspiration from Aittala et al. [2016] who extended the approach of Gatys et al. [2015] to generate svBRDF parameter maps from a single picture of a stationary material exemplar.

2.3 Spaces-of

Spaces of color [Nguyen et al. 2015], materials [Matusik 2003], textures [Matusik et al. 2005], faces [Blanz et al. 1999], human bodies [Allen et al. 2003], and more have been useful in graphics. Closest to our approach, Matusik et al. [2005] has devised a space of textures. Here, users can interpolate combinations of visually similar textures. They warp all pairs of exemplars to each other and constructs graph edges for interpolation when there is evidence that the warping is admissible. To blend between them, histogram adjustments are made. Consequently, interpolation between exemplars does not take a straight path in pixel space from one to the other, but traverses only valid regions. Photoshape [Park et al. 2019] learns the relation of given material textures over a database of 3D objects. Serrano et al. [2016] allow users to semantically control captured BRDF data. They represent BRDFs using the derived principal component basis [Matusik 2003] and map the first five PCA components to semantic attributes through learned radial basis functions. We take inspiration from this body of work and build a *continuous* space allowing SVBRDFs generation, interpolation and semantic control.

3 BACKGROUND

3.1 Flash Images

Aittala et al. [2016] leveraged the fact that a single flash image of a stationary material reveals multiple realizations of the same reflectance statistics under different light and view angles. We will now recall a simplified definition of their approach.

A flash image is an RGB image of a material, taken in conditions where a mobile phone’s flashlight is the dominant light source. We write $L(\mathbf{x})$ to denote the RGB radiance value at every image location \mathbf{x} . The image is assumed to be taken in —or converted to— linear space. The illumination is assumed to be an isotropic point light collocated with the camera. Further, the geometry is assumed to be flat and captured in a fronto-parallel setting, so that the direction

from light to every image location in 3D is known. Self-occlusion and parallax are assumed to be negligible.

Reflectance is parameterized by a *material*, represented as a function $f(\mathbf{x})$ mapping image location \mathbf{x} to shading model parameters, including the shading normal. Under these conditions, the reflected radiance is $L = \mathbf{R}f$, where \mathbf{R} is the *differentiable* rendering operator, mapping shading model parameters to radiance.

A material f explains a flash image L if it is *visually similar* to L when rendered. Unfortunately, without further constraints, there are many materials to explain the flash image. This ambiguity can be resolved when assuming that the material f is *stationary*. We say a material is stationary, if local statistics of the shading model parameters f do not change across the image.

Putting both —visual similarity and stationarity— together, the best material from a family f_θ of material mapping functions parameterized by a vector θ , can be found by minimizing a loss:

$$\mathcal{L}'(\theta) := \mathcal{T}(L, \mathbf{R}f_\theta) + \lambda \mathcal{S}(f_\theta), \quad (1)$$

where $\mathcal{T}(L, \mathbf{R}f_\theta)$ is a metric of visual similarity between a flash image L and a differentiable rendering $\mathbf{R}f_\theta$, and $\mathcal{S}(f)$ is a measure of stationarity of a material map f .

Comparison, \mathcal{T} , of two textures is not trivial. Pixel-by-pixel comparison is typically not suitable to evaluate visual statistical similarity. Instead, images are mapped to a feature space in which images that are perceived as similar textures, map to similar points [Portilla and Simoncelli 2000]. Different mappings are possible here. Classic texture synthesis [Heeger and Bergen 1995] uses moments of linear multi-scale filters responses. Gatys et al. [2015] proposed to use Gram matrices of non-linear multi-scale filters responses such as those of the VGG [Simonyan and Zisserman 2014] detection network. Such a characterization of textures was also used by Aittala et al. [2016] and, without loss of generality, will be used and extended in this work as well.

While f is stationary, L is not and has features at different random positions \mathbf{x} which are compared as

$$\mathcal{T}'(L_1, L_2) := \mathbb{E}_{\mathbf{x} \sim (0,1)^2, s \sim (0,1)} [|\mathcal{P}(L_1, \mathbf{x}) - \mathcal{P}(L_2, \mathbf{x})|_1], \quad (2)$$

where $\mathcal{P}'(L, \mathbf{x})$ crops a patch at the location \mathbf{x} resamples it to the input resolution of VGG [Simonyan and Zisserman 2014], computes the filter responses and ultimately their Gram matrices:

$$\mathcal{P}(L, \mathbf{x}) := \text{gram}(\text{vgg}(\text{resample}(\text{crop}(L, \mathbf{x}, s)))). \quad (3)$$

Here, s is a crop scale parameter chosen by the user.

Minimizing θ with respect to Eq. 1 for a given L results in a material. f_θ can represent different approaches. Aittala et al. [2016] directly use the pixel basis and optimize discrete material maps for θ using a single input flash image L . With their approach, optimizing for both visual similarity and stationarity is challenging. In particular, the reflectance stationarity term \mathcal{S} , requires a “spectral preconditioning” step as explained in their paper. Instead, we propose a novel approach in the form of a neural model f that is (i) defined on the entire infinite domain and (ii) is stationary by construction. Thus, our loss does not include the stationarity term.

Next, we describe how to generate RGB textures using deep learning (Sec. 3.2), before combining the two components (flash images and NN texture (spaces)) into our approach (Sec. 4).

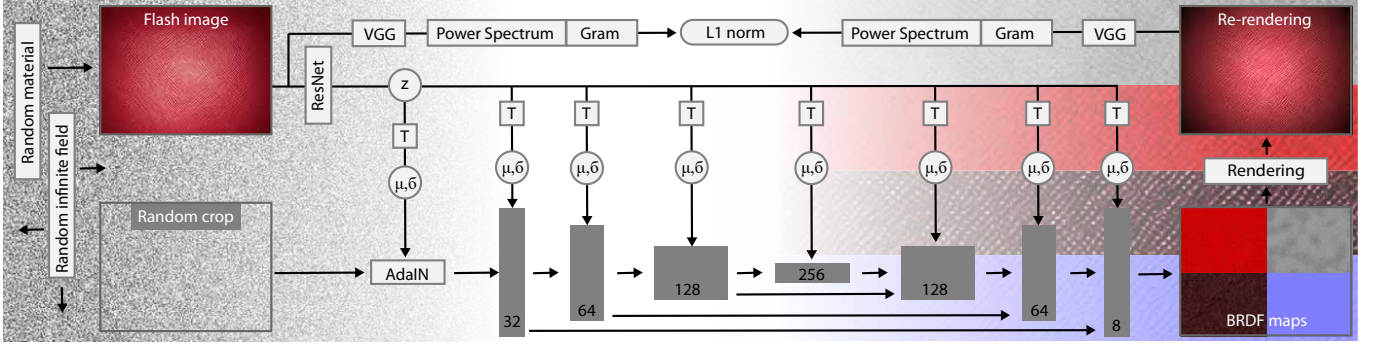


Fig. 3. **Our architecture.** Starting from an exemplar (**top-left**) training encodes the image to a compact latent space variable z . Additionally, a random infinite field is cropped with the same spatial dimensions as the flash input image. The noise crop is then reshaped based on a convolutional U-Net architecture. Each convolution in the network is followed by an Adaptive Instance Normalization (AdaIN) layer [Huang and Belongie 2017] reshaping the statistics (mean μ and standard deviation σ) of features. A learned affine transformation per layer maps z to the desired μ 's and σ 's. The output of the network are the diffuse, specular, roughness, normal parameters of a svBRDF that when rendered (using a flash light) look the same as the input.

3.2 Deep Texture Synthesis

Julesz [1965] define textures by their feature statistics across space. The choice of which features to use remains an important open problem. With the advent of deep learning, Gatys et al. [2015] suggested to use Gram matrices of these activations of filters, learned in deep convolutional neural networks (e.g., VGG [Simonyan and Zisserman 2014]), for neural style transfer. By optimizing directly over pixel values, their method can produce images with the desired texture properties. Aittala et al. [2016] rely on the same statistics to recover material parameters of stationary materials. These methods require a different optimization to be ran for each different material.

Another group of recent methods [Johnson et al. 2016; Ulyanov et al. 2016] introduce neural networks capable of producing RGB textures directly, in milliseconds. While these approach use a network to generate the textures, they are still limited to the input texture exemplar, and do not show further variations in their results. Ulyanov et al. [2017] introduced an explicit diversity term enforcing results in a batch to be different. This diversity is however limited and restrict the results quality. Indeed, they add a diversity term to the loss, but the architecture is not modified to enable it. Alternatively, adversarial training has been used to capture the essence of textures [Bergmann et al. 2017; Shaham et al. 2019], including the non-stationary case [Zhou et al. 2018] or even within a single image [Shaham et al. 2019]. In particular, StyleGAN [Karras et al. 2019] generates images with details by transforming noise using adversarial training. As opposed to these approach we do not rely on challenging adversarial trainings, by directly learning a Neural Network to produce VGG statistics.

Instead of incentivizing stationarity in the loss, Henzler et al. [2020] suggest a learnable texture representation that is built on mapping an infinite noise field to a field that has the statistics of the exemplar texture. Their method is a point operation, implemented by an MLP that is fed exclusively with noise sampled at different scales as done by Perlin [1985]. By explicitly preventing the network to access any absolute position, this approach is stationary by-design.

4 NOISE TO BRDF TEXTURE SPACES

An overview of our approach is shown in Fig. 3. We train a neural network which acts as a decoder $f_\theta(\mathbf{x}|z)$ that generalizes across spatial positions \mathbf{x} as well as across materials, expressed as latent material codes z . The material codes z are produced by an encoder g with $z = g(L)$. Both encoder and decoder are trained jointly over a set of flash images using the loss:

$$\mathcal{L}(\theta) := \mathbb{E}_L[\mathcal{T}(L, \mathbf{R}f_\theta(\cdot|g_\theta(L)))]. \quad (4)$$

This equation is an adapted version of Eq. 1 to fit our objectives. In particular we propose a neural network-based f_θ , leveraging the expectation \mathbb{E}_L over all flash images in our training set and removing the stationarity term as it is enforced by construction in our network architecture. We describe the flash image encoder g (Sec. 4.1), the material texture decoder f (Sec. 4.2) and the texture comparison model \mathcal{T} (Sec. 4.3), next.

4.1 Encoder

The encoder g maps a flash image L to a latent code z . It is implemented using ResNet-50 [He et al. 2016]. The ResNet starts at a resolution of 512×384 and maps to a compact latent code. Empirically, we find a $n_z = 64$ -dimensional latent space to work best for our data and present all results using this number.

4.2 Decoder

The decoder f maps location \mathbf{x} , conditioned on a material code z to a set of material parameter maps. The key idea is to provide the architecture with access to noise, as previously done for style transfer [Huang and Belongie 2017], generative modelling [Karras et al. 2019] or 3D texturing [Henzler et al. 2020]. In particular, we sample rectangular patches with edge length of $n \times m$ pixels from an infinite random field and convert them to material maps using a U-net architecture [Ronneberger et al. 2015]. The U-net starts at the desired output resolution $n \times m$ and reduces resolution four times using max-pooling before bilinearly upsampling $n \times m$ again. Let F be the array of input features. For $i = 0$, the first level, in full resolution, these features are sampled from the random field at \mathbf{x} .

Then the output features F' are

$$F' := \text{adaIN}(\text{conv}_\theta(F), T_\theta z), \quad (5)$$

where adaIN is Adaptive Instance Normalization (AdaIN) [Huang and Belongie 2017], conv a convolution (including up- or down-sampling and ReLU non-linearity) and T is an affine transformation. Components with learned parameters are denoted with subscript θ .

We use AdaIN as defined by Huang and Belongie [2017] as

$$\text{adaIN}(\xi, \{\mu, \sigma^2\}) = \frac{\sigma}{\sigma_F} (\xi - \mu_F) + \mu \quad (6)$$

and remaps the input features with mean μ_F and variance σ_F^2 to a distribution with mean μ and variance σ^2 .

The affine mapping T is implemented as $(n_z + 1) \times (2 \times c_i)$ matrices multiplied with the latent code – augmented with a 1 in dimension $n_z + 1$. Here $2 \times c_i$ represent a different mean and variance for each channel dimension c_i of a layer. It provides the link between the material code and the noise statistics. Each material code z is mapped to a mean and variance to control how the statistics of features are shaped at every channel on every layer of the decoder. Our control of noise statistics from latent codes is similar to StyleGAN [Karras et al. 2019], with the key difference that we do not sample noise at different scales, but learn how to produce noise with different, complex, characteristics at different scales by repeatedly filtering it from high resolutions.

4.3 Images Comparison

We propose to compare images based on a loss that accounts both for the statistics of activations [Gatys et al. 2015] and their spectrum [Liu et al. 2016] on multiple scales across the infinite spatial field,

$$\mathcal{T}(L_1, L_2) := \mathbb{E}_{x \sim \mathbb{R}^2, s \sim (s_{\min}, s_{\max})} [|\mathcal{P}(L_1, x, s) - \mathcal{P}(L_2, x, s)|_1]. \quad (7)$$

$$\mathcal{P}(L, x, s) := \text{gram}(V) + \lambda \cdot \text{powerSpectrum}(V) \quad (8)$$

$$V := \text{vgg}(\text{resample}(\text{crop}(L, x, s))) \quad (9)$$

Spectrum. VGG Gram matrices capture the frequency of a feature appearance, unless it forms a regular pattern [2016]. Liu et al. [2016] proposed to include the L1 norm of the power spectra of two RGB images into the texture metric for learning a single texture. We therefore combine both ideas and use VGG, but do not limit ourselves to its statistics, and also leverage its spectrum.

Scale. As VGG works at a specific scale of features it was trained for, it behaves differently at different scales. As the material should be visually plausible regardless of its scale we include multiple scales s , ranging from $s_{\min} = 0$ to $s_{\max} = 8$ in the loss computation.

Infinity. Expectation over the infinite plane is implemented by simply training with different random seeds for the noise field. This results in the generation of statistically similar, but locally different variations of materials. As, given a seed, every generated patch is a coherent material, combinations of multiple patches remains coherent as well. This allows to query an endless, seamless and diverse stream of patches without repetition. It also avoids to overfit and is crucial to guarantee stationarity by-design.

4.4 Material model

We use the Cook-Torrance [1982] micro-facet BRDF Model, with Smith’s geometric term [Heitz 2014], Schlick’s [1994] Fresnel and GGX [Walter et al. 2007]. Hence, parameters are diffuse albedo, specular albedo, roughness and height, i.e., eight dimensions. For practical purposes we differentiate height into normal vectors.

4.5 Alignment

Many flash images entail a slight rotation as it can be difficult to take a completely fronto-parallel image. This was handled by Aittala et al. [2016] by locating the brightest pixel and cropping, but we found our, more abstract, training to struggle with such a solution.

Instead, we add a horizontal and a vertical rotation angle to the parameter vector generated from the latent code (not shown in Fig. 3 for clarity). During training, these are used to rotate the plane, including the normals. During testing, these angles are not applied meaning that the output is in the local space of the exemplar.

We use a branch of the encoder to perform the alignment task, allowing to jointly align all images based on their visual features.

A byproduct is that the encoder returns angular distance to fronto-parallelity, which could be used to guide users during capture.

4.6 Training

For better generalization, we train the system as a Variational Auto-encoder (VAE) [Kingma and Welling 2013], so instead of mapping to a single 64-D latent material code, the encoder g maps to a 64-D mean and variance vector, from which we sample in training. At test time we use the mean for each 64-D. We have omitted the additional VAE terms enforcing z to be normally distributed from Eq. 4 and Fig. 3 for clarity. We trained our model for 4 days, with a batch size of 4 on a NVIDIA Tesla V100 using the ADAM optimizer with a learning rate of $1e-4$ and weight decay $1e-5$.

4.7 Semantic Control

Our approach allows to embed flash pictures into material codes that can be decoded to corresponding materials. Furthermore, every latent material code results in a plausible material. Yet this is not enough for intuitive manipulation. Given a material code z , we now explore how we can modify it to perform high level semantic control, e.g., making a material more leather-like.

We manually label our dataset with the classes wood, leather, stone, fabric, metal, rubber, dirty, paint, and plastic. For every class C we compute the direction \mathbf{n}_C in latent space that is normal to a plane best separating the in-class and out-class exemplars. If C is the set of all exemplar indices in the class, this is

$$\mathbf{n} = \mathbb{E}_{i \in C} [z] - \mathbb{E}_{i \notin C} [z] \quad (10)$$

a vector pointing from the barycenter of class C to the barycenter of the non-class. This allows to relate semantic parameters to a position in the latent space. For a material with code z to become “more like C ”, it is changed to $z + \alpha \mathbf{n}_C$, where α is a user control.



Fig. 4. **Infinite spatial extent.** Our learned BRDF space can be sampled at any query (x,y) location without producing visible repetition artifact. The network architecture, by construction, does not require any special boundary alignment to avoid tiling artifacts. All results are sampled from the learned BRDF space.

5 RESULTS

5.1 Dataset

We created an extended dataset of flash images for testing and training of our approach. It comprises of 356 images of various types of materials we captured using smartphones. We reserve 50 images for testing, augmented by all images from Aittala et al. [2016]. Hence, no image from Aittala et al. [2016] was seen during training. For our control experiment, we leverage the semantic labels described in Sec. 4.7.

5.2 Quantitative Evaluation

For quantitative analysis we compare our approach to a range of alternative methods with respect to different metrics.

Methods. We compare to three methods by (i) Aittala et al. [2016], (ii) Deschaintre et al. [2018], and (iii) Zhao et al. [2020]. All methods were applied to our test data and re-rendered under the same lighting conditions with the material model described in their respective paper. Examples are shown in Fig. 5.

Metrics. We quantify *style*, *diversity*, and *computational speed*. Style is captured by L1 difference of the VGG Gram matrices of

Table 1. Comparison of different methods.

Method	Style Error	Diversity	Time
Aittala et al. [2016]	1.25	0	<1h
Deschaintre et al. [2018]	1.0	0	<0.5s
Zhao et al. [2020]	1.01	0	<1h
Ours	0.66	0.43	<0.2s

rendered images. A good agreement in style has a low number i.e., less is better. Diversity is captured as the mean pairwise VGG L1 across all realizations. Here, more is better. Finally, we measure compute time, where less is better.

Results. Results are shown in Fig. 7. We see that our method shows lower style error than other approaches, including Deschaintre et al. [2018] which decompose individual exemplars into shading channels. The approach of Zhao et al. [2020] and Aittala et al. [2016], which target a closer objective to ours, statistical reproduction of a material, but demonstrate higher style error.

Note, that only our approach and Aittala et al. [2016] produce a stationary result. Only our result is diverse, i.e., we produce infinitely many realizations of a texture while all other approaches produce

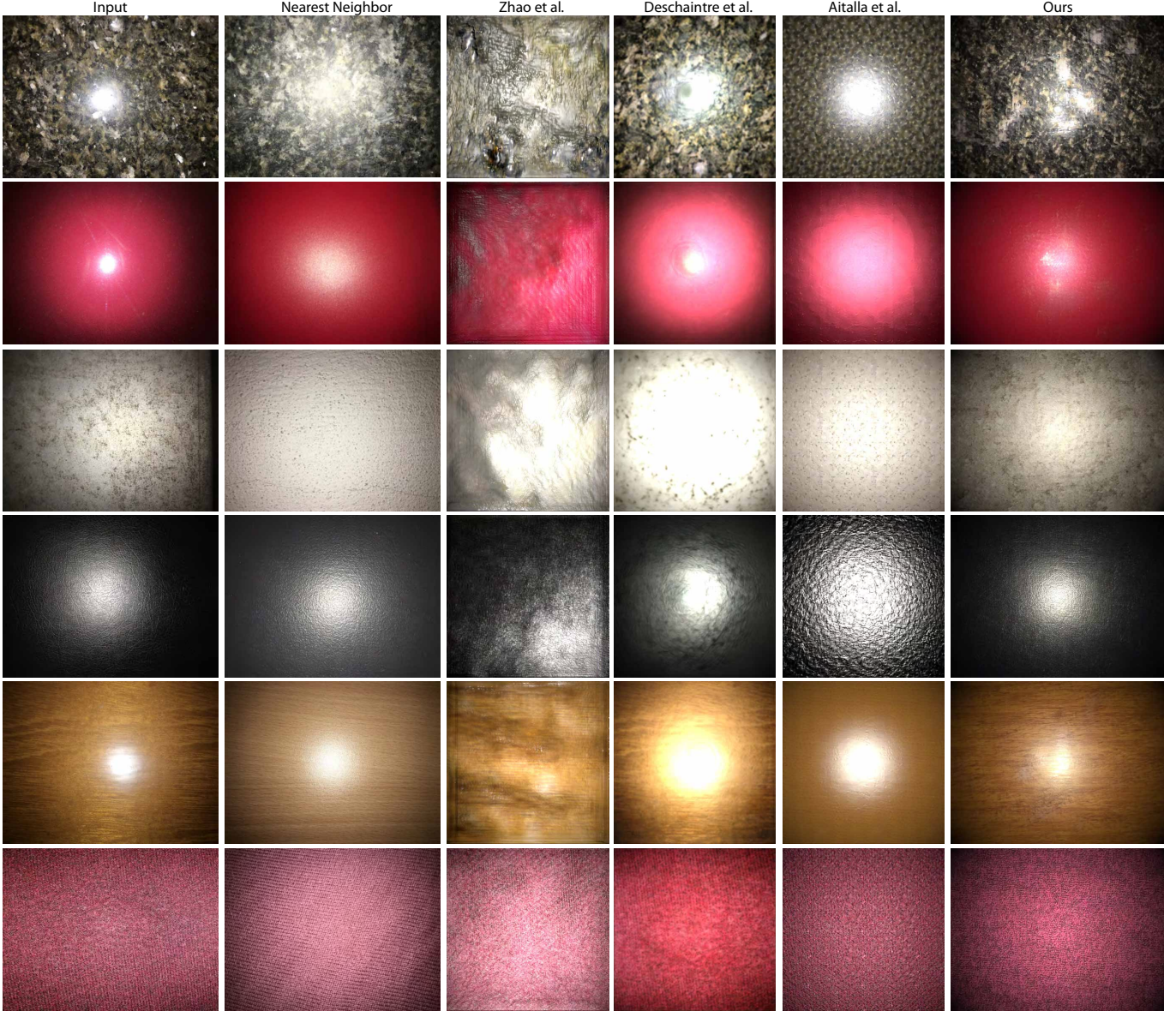


Fig. 5. **Comparison with competitors.** Comparison of our results to methods that decompose an image into svBRDF parameters (**columns**) for different flash input images (**rows**). Nearest Neighbor (NN) recovers the closest material in our training set in terms of style. Note that Deschaintre et al. [2018] additionally require 4-channel BRDF measurements for training, while Zhao et al., Aittala et al. and ours can operate directly on flash images. However, Zhao et al. and Aittala et al. are overfitted to single exemplars whereas our method is able to re-synthesis unseen flash images from our test data set.

only one. Thus, diversity is zero for all other, while it is a constant for ours. We summarize this in Tbl. 1.

In terms of computational speed, Aittala et al. [2016] and Zhao et al. [2020] both require around one hour of compute time for each per-exemplar optimization to produce a stationary texture. Deschaintre et al. [2018] is as fast as our approach (less than 0.5s), executing only a decoder, but do not produce a stationary texture.

Our approach benefits from the same speed and allows to generate diverse, infinite materials. We measured an average speed per forward pass of 0.196s over all test steps.

5.3 Qualitative Evaluation

Decomposition. Qualitative examples of our decomposition are depicted in Fig. 6. We see that our approach captures a range of different materials, reproducing the style, yet being diverse to produce an infinite field of values as shown in Fig. 4.

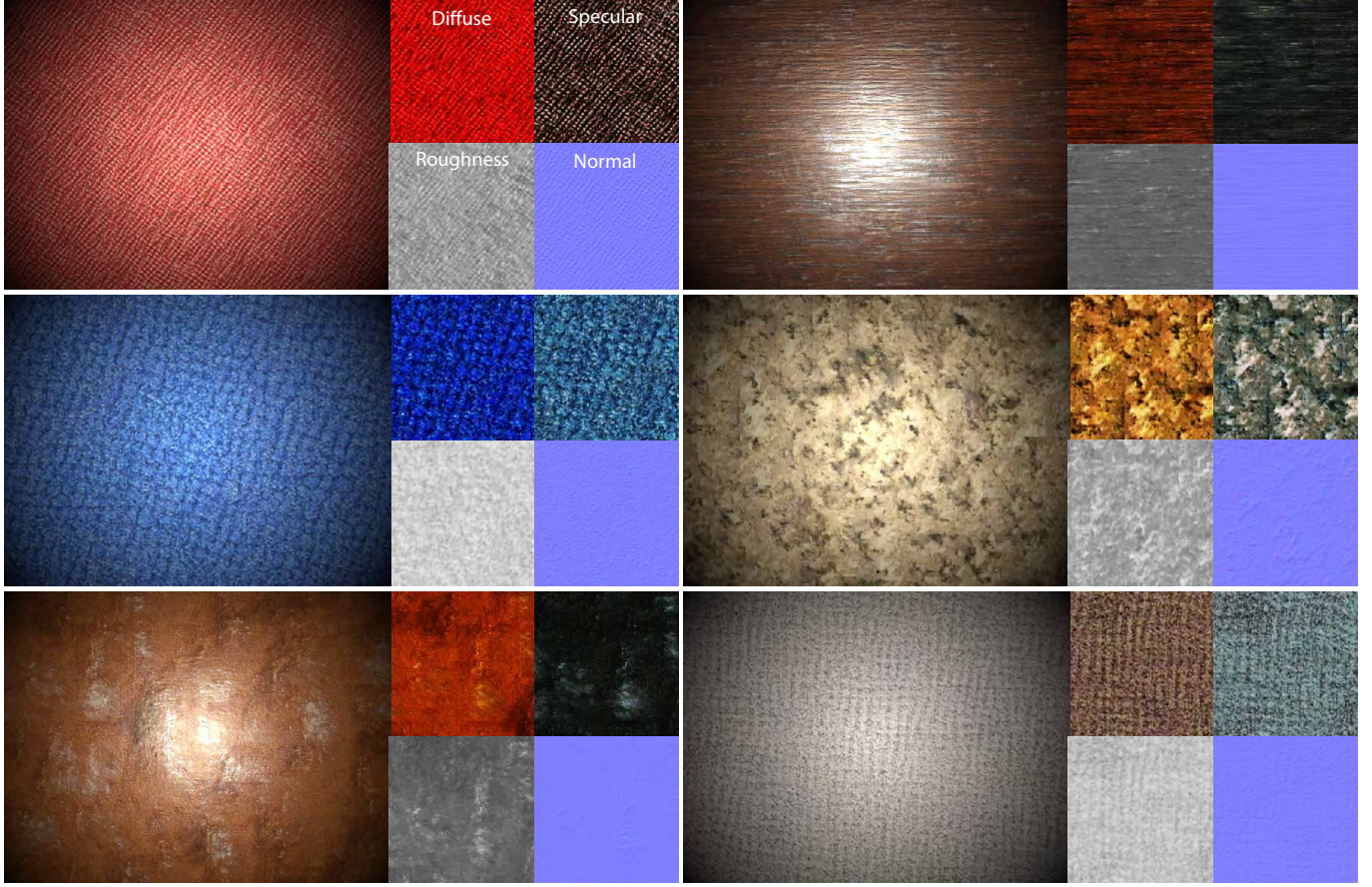


Fig. 6. **Qualitative results.** Result produced by our method for six materials. For each material, we show the re-rendering left, followed by insets showing crops of the diffuse, specular, roughness, and normal channel. At inference time, our network runs at 200 ms.

Interpolation. Interpolation of latent BRDF texture codes is shown in Fig. 8. Please see the captions for additional discussion.

Semantic control. Fig. 9 shows an application exploring the latent space with semantic controls. Please see the caption for a discussion.

Texturing. Fig. 1 shows examples of applying maps produced by our approach to a complex 3D shape. Thanks to our generative

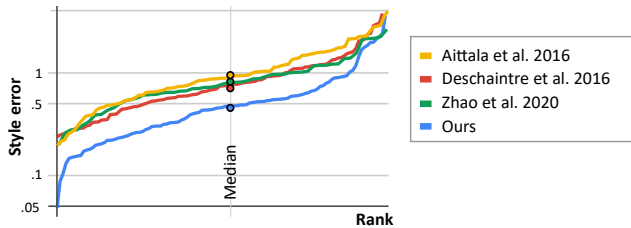


Fig. 7. Ordered error (Zipf) plot comparing four methods (colors). Each curve is produced by sorting the errors of each method. The median can be compared in the middle. The vertical axis is logarithmic style error, less is better. The horizontal axis is rank (low error left, high error right).

model, we can produce an endless stream of sneakers, without spatial or material repetition. At any point, a user can perform semantic control using our space, randomize the generated material, generate new materials from pictures or interpolate between new materials and old ones.

Generation. As any point in our space is a material, we can simply sample randomly to produce a coverage of all materials available in the space. Fig. 10 shows random samples from this space applied to a set of 3D cubes. Note that no materials are similar and all look plausible, with spatially varying appearance.

Interactive demo. The visual quality is best inspected from our interactive WebGL demo in the supplemental. It allows exploring the space by relighting, changing the random seed and visualizing individual BRDF model channels and their combinations. The same package contains all channels of all materials as images. See the accompanying video for a demonstration of our interactive interface.

6 USER EXPERIMENT

We perform a user experiment to better understand the properties of our method, in particular we ask three questions: (i) Is a semantic

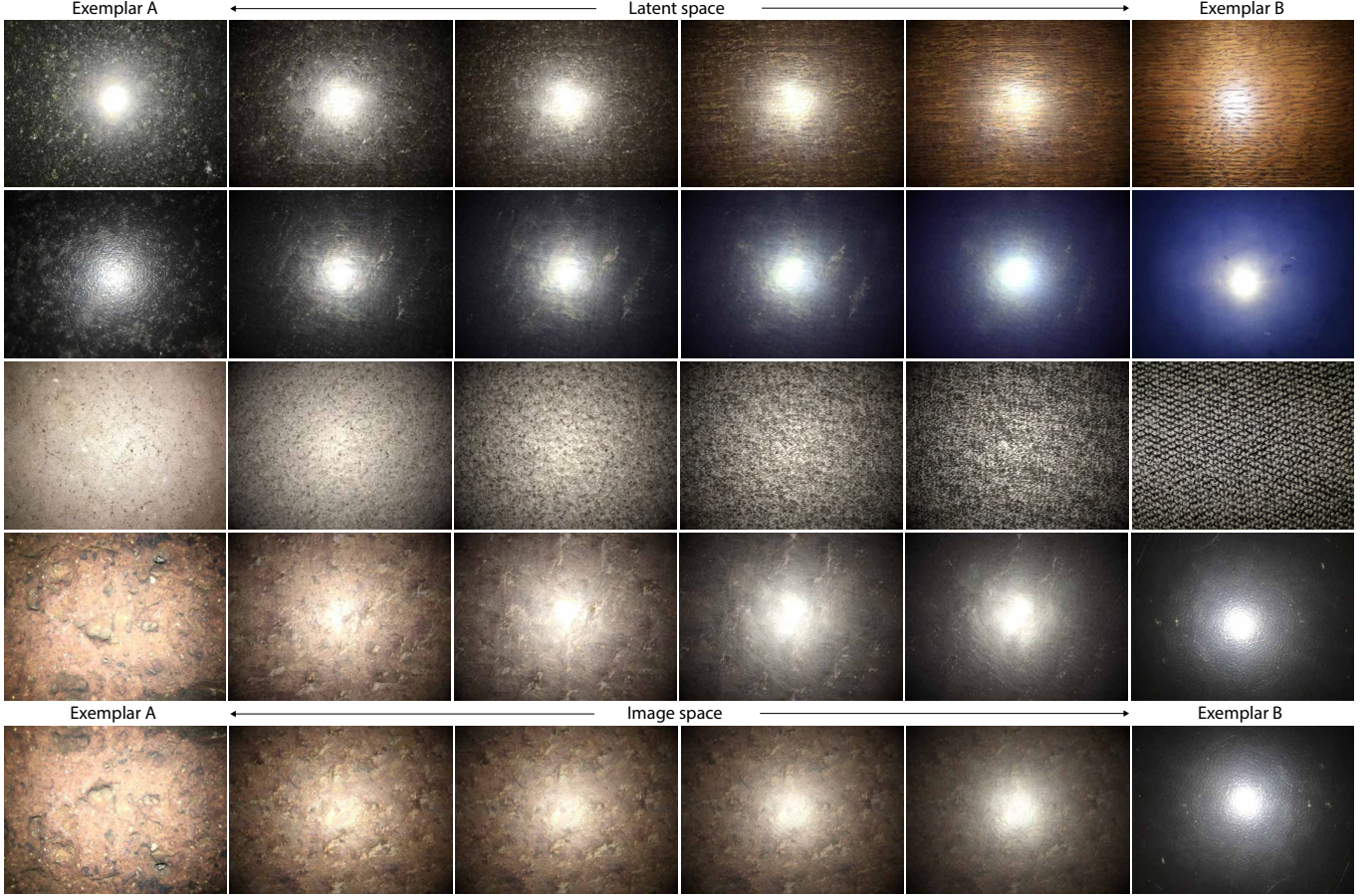


Fig. 8. **Interpolation of latent BRDF texture codes.** In each row, a left and a right latent code z_1 and z_2 are obtained by encoding two flash images, respectively. The intermediate, continuous field of BRDF parameters is computed by interpolating, in the learned BRDF space, from z_1 to z_2 and conditioning the decoder Convolutional Neural Network (CNN) with the intermediate code. The result is lit with a fronto-parallel light source to demonstrate the changes in appearance. For comparison, the last row shows image space linear interpolation – compare against the second last row showing latent space interpolation.

change in our space would be recognized as such? (ii) Is our semantic labeling is consistent with the one of users? (iii) Which method result (between [Aittala et al. 2016; Deschaintre et al. 2018; Zhao et al. 2020] and ours) is most similar to the input flash picture?

Methods. Subjects (Ss) anonymously completed an online form without time limit. Secondary variables relating to experience and task difficulty were recorded. The form was composed of three parts.

The first part was showing 10 pairs of rendering of materials. One random image in the pair was a re-synthesis from a flash image input, the other a re-synthesis from the same image, but changed by a unit step into the direction of a semantic class. In a Two-alternative Forced Choice (2AFC), Ss were asked to indicate which of the images is semantically more similar to the label.

The second part presented 20 images and Ss had to choose from the list of our materials classes (Fabric, Leather, Metal, Paint, Plastic, Stone, Wood) which class this material belongs to.

In the third part, 12 sets of five images each were shown, where the first one was marked the reference and the four others are re-synthesis result by four other methods (Deschaintre et al. [2018], Aittala et al. [2016] and Zhao et al. [2020]), shown in random order. Ss were asked to say which result was matching the reference best.

Analysis. We performed a binomial and t -tests between between the hypothesis that Ss answered randomly resp. they had identical preferences. Effect size for correct/incorrect and preference answers is reported as percentage. A total of $N = 57$ Ss completed the experiment. They quantified their own experience in Computer Graphics as 3.06, in general science as 3.39, and in the arts as 2.86 on a five-point Likert scale.

Results. For the first task, we can reject ($p < .001$, binomial test) the null-hypothesis that Ss randomly choose which result is changed along a semantic axis. On average, Ss identified the correct class in 82.9 % of the cases. The material class working best is fabric at 100 %, followed by leather at 95 % and wood at 96.92 %, trailed by



Fig. 9. **Semantic control.** After a flash exemplar (**first column**) has been embedded into our learned BRDF space (**second column**), its latent material code can be manipulated such that certain semantic attributes are enhanced or suppressed (**last three columns**). Note, that the semantic change maximizes the attribute, while retaining properties not in conflict. A move towards fabric in the first and fourth example, makes both become more like fabric, (e.g., less shiny) but retains color. A move towards rubber imposes some structure to the normal map, but is compatible with both shiny and rough.

paint at 63.43 % and stone at 60.47 % (all classes $p < .001$, binomial test). Ss rated the difficulty of this task as 2.91 on a five-point Likert scale. This indicates that moving along a semantic axis in our space correlates with the semantic classification of users, a choice they report being confident about.

From the second task, we can also reject ($p < .0001$, binomial test) the null-hypothesis that Ss pick a semantic class randomly. On average, subjects agreed to our classification in 68.8 % of the cases. Difficulty of this task was rated at 3.0 on the same five-point Likert

scale. This indicates that our semantic labeling is in agreement with the Ss' choices which they also felt confident to make.

The third task allows comparing methods against each other. Our method is significantly ($p < .001$, t -test) preferred over all others when it was chosen best in 47.7% of the cases, followed by Deschaintre et al. [2018] at 23.6 %, Aittala et al. [2016] at 19.3% and Zhao et al. [2020] at 9.2 %. This task was rated difficult at 3.17 on said scale. All this indicates, that participants have preferences between methods in our favor while reporting to understand the task.



Fig. 10. Random samples from the space of all materials.

7 CONCLUSION

We have presented an approach to generate a space of BRDF textures using a small set of flash images in an unsupervised way. Comparing this approach to the literature shows competitive metrics for re-renderings with the unique advantage of being able to generate an infinite and diverse field of BRDF parameters.

In future work, more refined differentiable rendering material models could be used to derive stochastic textures, including shadows, displacement, or scattering as well as volumetric or time-varying textures. We believe that our framework will represent a stepping stone for more complex infinite and diverse BRDFs acquisition as well as their semantic manipulation.

REFERENCES

- Miika Aittala, Timo Aila, and Jaakko Lehtinen. 2016. Reflectance modeling by neural texture synthesis. *ACM Trans Graph (Proc. SIGGRAPH)* 35, 4 (2016), 65.
- Brett Allen, Brian Curless, and Zoran Popović. 2003. The space of human body shapes: reconstruction and parameterization from range scans. *ACM Trans Graph (Proc. SIGGRAPH)* 22, 3 (2003), 587–94.
- Connelly Barnes, Eli Shechtman, Adam Finkelstein, and Dan B Goldman. 2009. Patch-Match: A randomized correspondence algorithm for structural image editing. *ACM Trans Graph (Proc. SIGGRAPH)* 28, 3 (2009), 24.
- Urs Bergmann, Nikolay Jetchev, and Roland Vollgraf. 2017. Learning texture manifolds with the periodic spatial GAN. In *J MLR*. 469–477.
- Volker Blanz, Thomas Vetter, et al. 1999. A morphable model for the synthesis of 3D faces. In *Siggraph*, Vol. 99. 187–194.
- Robert L Cook and Tony DeRose. 2005. Wavelet noise. *ACM Trans Graph* 24, 3 (2005), 803–11.
- Robert L Cook and Kenneth E Torrance. 1982. A reflectance model for computer graphics. *ACM Trans Graph* 1, 1 (1982), 7–24.
- Valentin Deschaintre, Miika Aittala, Frédo Durand, George Drettakis, and Adrien Bousseau. 2018. Single-image svbrdf capture with a rendering-aware deep network. *ACM Trans Graph (Proc. SIGGRAPH)* 37, 4 (2018), 128.
- Valentin Deschaintre, Miika Aittala, Frédo Durand, George Drettakis, and Adrien Bousseau. 2019. Flexible SVBRDF Capture with a Multi-Image Deep Network. *Comp Graph Forum* 38, 4 (2019), 1–13.
- Alexei A Efros and Thomas K Leung. 1999. Texture synthesis by non-parametric sampling. In *ICCV*, Vol. 2.
- Duan Gao, Xiao Li, Yue Dong, Pieter Peers, Kun Xu, and Xin Tong. 2019. Deep inverse rendering for high-resolution SVBRDF estimation from an arbitrary number of images. *ACM Trans Graph (Proc. SIGGRAPH Asia)* 38, 4 (2019), 134.
- Leon Gatys, Alexander S Ecker, and Matthias Bethge. 2015. Texture synthesis using convolutional neural networks. In *NIPS*.
- Stamatis Georgoulis, Konstantinos Rematas, Tobias Ritschel, Efstratios Gavves, Mario Fritz, Luc Van Gool, and Tinne Tuytelaars. 2017. Reflectance and natural illumination from single-material specular objects using deep learning. *PAMI* 40, 8 (2017), 1932–1947.
- Darya Guarnera, Giuseppe Claudio Guarnera, Abhijeet Ghosh, Cornelia Denk, and Mashhuda Glencross. 2016. BRDF representation and acquisition. In *Comp Graph Forum*, Vol. 35. 625–650.
- Yu Guo, Cameron Smith, Miloš Hašan, Kalyan Sunkavalli, and Shuang Zhao. 2020. MaterialGAN: Reflectance Capture using a Generative SVBRDF Model. *ACM Trans Graph* 39, 6 (2020).
- Kaiming He, Xiangyu Zhang, Shaoqing Ren, and Jian Sun. 2016. Deep residual learning for image recognition. In *CVPR*. 770–8.
- David J Heeger and James R Bergen. 1995. Pyramid-based texture analysis/synthesis. In *Proc. SIGGRAPH*. 229–38.
- Eric Heitz. 2014. Understanding the masking-shadowing function in microfacet-based BRDFs. (2014).
- Philipp Henzler, Niloy J Mitra, and Tobias Ritschel. 2020. Learning a Neural 3D Texture Space from 2D Exemplars. *CVPR* (2020).
- Xun Huang and Serge Belongie. 2017. Arbitrary style transfer in real-time with adaptive instance normalization. In *ICCV*. 1501–10.
- Phillip Isola, Jun-Yan Zhu, Tinghui Zhou, and Alexei A Efros. 2016. Image-to-Image Translation with Conditional Adversarial Networks. *arxiv* (2016).
- Justin Johnson, Alexandre Alahi, and Li Fei-Fei. 2016. Perceptual losses for real-time style transfer and super-resolution. In *ECCV*.
- Bela Julesz. 1965. Texture and visual perception. *Scientific American* 212, 2 (1965).
- Tero Karras, Samuli Laine, and Timo Aila. 2019. A style-based generator architecture for generative adversarial networks. In *CVPR*. 4401–10.
- Diederik P Kingma and Max Welling. 2013. Auto-encoding variational bayes. *arXiv preprint arXiv:1312.6114* (2013).
- Alexandr Kuznetsov, Milos Hasan, Zexiang Xu, Ling-Qi Yan, Bruce Walter, Nima Khademi Kalantari, Steve Marschner, and Ravi Ramamoorthi. 2019. Learning generative models for rendering specular microgeometry. *ACM Trans Graph (Proc. SIGGRAPH Asia)* 38, 6 (2019).
- Vivek Kwatra, Irfan Essa, Aaron Bobick, and Nipun Kwatra. 2005. Texture optimization for example-based synthesis. In *ACM Trans Graph*, Vol. 24.
- Xiao Li, Yue Dong, Pieter Peers, and Xin Tong. 2017. Modeling surface appearance from a single photograph using self-augmented convolutional neural networks. *ACM Trans Graph* 36, 4 (2017), 45.
- Zhengqin Li, Kalyan Sunkavalli, and Manmohan Chandraker. 2018a. Materials for masses: SVBRDF acquisition with a single mobile phone image. In *ECCV*. 72–87.
- Zhengqin Li, Zexiang Xu, Ravi Ramamoorthi, Kalyan Sunkavalli, and Manmohan Chandraker. 2018b. Learning to reconstruct shape and spatially-varying reflectance from a single image. In *SIGGRAPH Asia 2018*. ACM, 269.
- Guilin Liu, Duygu Ceylan, Ersin Yumer, Jimei Yang, and Jyh-Ming Lien. 2017. Material editing using a physically based rendering network. In *ICCV*. 2261–2269.
- Gang Liu, Yann Gousseau, and Gui-Song Xia. 2016. Texture synthesis through convolutional neural networks and spectrum constraints. In *ICPR*. 3234–9.
- Benoit B Mandelbrot. 1983. *The fractal geometry of nature*. Vol. 173. WH Freeman New York.
- W Matusik. 2003. A data-driven reflectance model. *ACM Trans Graph* 22, 3 (2003), 759–769.
- Wojciech Matusik, Matthias Zwicker, and Frédo Durand. 2005. Texture design using a simplicial complex of morphable textures. *ACM Trans Graph (Proc. SIGGRAPH)* 24, 3 (2005).
- Chuong H Nguyen, Tobias Ritschel, and Hans-Peter Seidel. 2015. Data-driven color manifolds. *ACM Trans Graph* 34, 2 (2015), 20.
- Keunhong Park, Konstantinos Rematas, Ali Farhadi, and Steven M Seitz. 2019. Photo-shape: photorealistic materials for large-scale shape collections. *ACM Transactions on Graphics (TOG)* 37, 6 (2019), 192.
- Ken Perlin. 1985. An Image Synthesizer. *SIGGRAPH Comput. Graph.* 19, 3 (1985).
- Bui Tuong Phong. 1975. Illumination for computer generated pictures. *Commun. ACM* 18, 6 (1975), 311–317.
- Javier Portilla and Eero P Simoncelli. 2000. A parametric texture model based on joint statistics of complex wavelet coefficients. *Int J Comp Vis* 40, 1 (2000), 49–70.
- K. Rematas, T. Ritschel, M. Fritz, E. Gavves, and T. Tuytelaars. 2016. Deep Reflectance Maps. In *CVPR*.
- Olaf Ronneberger, Philipp Fischer, and Thomas Brox. 2015. U-net: Convolutional networks for biomedical image segmentation. In *MICCAI*. 234–41.
- Christophe Schlick. 1994. An inexpensive BRDF model for physically-based rendering. In *Comp Graph Forum*, Vol. 13. 233–246.
- Christopher Schwartz, Ralf Sarlette, Michael Weinmann, and Reinhard Klein. 2013. DOME II: A Parallelized BTF Acquisition System. In *MAM*. 25–31.
- Omry Sendik and Daniel Cohen-Or. 2017. Deep correlations for texture synthesis. *ACM Trans Graph* 36, 5 (2017), 161.
- Ana Serrano, Diego Gutierrez, Karol Myszkowski, Hans-Peter Seidel, and Belen Masia. 2016. An intuitive control space for material appearance. *ACM Trans Graph (Proc. SIGGRAPH Asia)* 35, 6 (2016).
- Tamar Rott Shaham, Tali Dekel, and Tomer Michaeli. 2019. Singan: Learning a generative model from a single natural image. In *ICCV*.

- Karen Simonyan and Andrew Zisserman. 2014. Very deep convolutional networks for large-scale image recognition. *arXiv preprint arXiv:1409.1556* (2014).
- Dmitry Ulyanov, Vadim Lebedev, Andrea Vedaldi, and Victor S Lempitsky. 2016. Texture Networks: Feed-forward Synthesis of Textures and Stylized Images.. In *ICML*. 4.
- Dmitry Ulyanov, Andrea Vedaldi, and Victor Lempitsky. 2017. Improved texture networks: Maximizing quality and diversity in feed-forward stylization and texture synthesis. In *CVPR*.
- Bruce Walter, Stephen R Marschner, Hongsong Li, and Kenneth E Torrance. 2007. Microfacet models for refraction through rough surfaces. In *Proc. EGSR*. 195–206.
- Li-Yi Wei and Marc Levoy. 2000. Fast texture synthesis using tree-structured vector quantization. In *Proc. SIGGRAPH*.
- Yezi Zhao, Beibei Wang, Yanning Xu, Zheng Zeng, Lu Wang, and Nicolas Holzschuch. 2020. Joint SVBRDF Recovery and Synthesis From a Single Image using an Unsupervised Generative Adversarial Network. In *EGSR*.
- Yang Zhou, Zhen Zhu, Xiang Bai, Dani Lischinski, Daniel Cohen-Or, and Hui Huang. 2018. Non-stationary texture synthesis by adversarial expansion. *arXiv preprint arXiv:1805.04487* (2018).